Journal of Basics and Applied Sciences Research (JOBASR)
ISSN (print): 3026-9091, ISSN (online): 1597-9962
Volume 2(4) December 2024
DOI: https://doi.org/10.33003/jobasr-2024-v2i4-63

Tuning ZnO with Al and B Doping for Efficient Solar Cell Windows

Ewansiha Kingsley Osarumwense[1,3]*, Yabagi Jibrin Alhaji [1], Ladan Muhammed Bello [1], Nmaya Mohammed Mohammed [1] and Kimpa Mohammed Isah [2]
[1]Department of Physics, Ibrahim Badamasi Babangida University, Lapai, Niger State.
[2]Department of Physics, Federal University of Technology Minna, Niger State
[3]Department of Physics, Federal Polytechnics Bida, Niger State
*Corresponding Author Email: kingsleyewansiha74@gmail.com

ABSTRACT
This study investigates the structural properties of ZnO, ZnO:Al, ZnO:B, and ZnO:Al:B nanoparticles synthesized via the sol-gel method for potential application as window layers in solar cells. X-ray diffraction (XRD) analysis reveals the crystalline structure, phase composition, crystallite size, and lattice parameters of the synthesized materials. Doping with aluminum (Al) and boron (B) induces significant changes in the lattice parameters, crystallinity, and crystallite size. The XRD patterns demonstrate a hexagonal wurtzite structure for all samples, with shifts in peak positions and broadening indicating lattice distortions and defects. The findings provide valuable insights into the effects of Al and B doping on the structural properties of ZnO nanoparticles, contributing to the optimization of ZnO-based materials for photovoltaic applications.

Keywords:
Zinc oxide (ZnO),
Nanoparticles,
Solar cells.

INTRODUCTION

The widespread use of photovoltaics (PV) to convert sunlight into electricity has proven to be effective in absorbing solar light. Solar cells, which are crucial to this, are used to achieve this. In the past, silicon (Si) was the preferred material for the absorber layer found in solar cells. On an industrial scale, this led to the creation of the first generation of solar cells. In spite of this, more advanced materials have been created, most notably copper indium gallium selenide (CIGSe) and cadmium telluride (CdTe), which are also more appealing substitutes for Si in terms of their essential characteristics (Regmi et al., 2023). Since there are materials other than silicon that can be used, one of the most important problems is figuring out how to maximize the amount of sunlight that reaches the absorber layer in order to quantify charge carriers, which are then used to reduce electrical energy. To perform this purpose, an efficient transparent conducting layer (TCO), typically composed of oxide materials, is needed (Jang et al., 2023). The application of TCOs, or transparent conductive oxides, is very important. Because of their special combination of optical transparency and electrical conductivity, they are frequently used as electrical contacts for solar cells and light-emitting diodes (Speaks, 2020). As a result, the most popular choices for industrial TCO are indium tin oxide (ITO) and fluorine-doped tin oxide (FTO). This is because of its very high transmission, high conductivity, low light absorption, low refractive index, high stability, and toughness (Chavan et al., 2023). However, alternative TCO materials have become necessary because of the high cost and possible health risks of indium, as well as the challenge of using fluorine in FTO deposition. The development of highly oriented and transparent ZnO thin films has attracted a lot of attention recently due to its potential uses in information technology, biosensors, field emitters, photodetectors, ultraviolet laser emission, field emitters, window layer for solar cells, piezoelectricity, and short wavelength light emitting diodes (Khan et al., 2011). Zinc oxide films (ZnO) have become the focus of attention of researchers as promising materials that can replace popular TCOs in the PV market. It is a versatile material that finds applications in various products (Khantoul et al., 2018). Because of its many desirable qualities, such as its low cost, lack of toxicity, abundance of resources, superior chemical and thermal stability, and resistance to hydrogen plasma treatment, zinc oxide (ZnO) has become increasingly popular (Ibrahim et al., 2013). Technologically speaking, zinc oxide-based materials are the most intriguing due to their unique

characteristics, which include a broad direct band gap of approximately 3.37 eV, a semiconductor material with a high exciton binding energy of 60 meV at room temperature, and crystallization in the standard hexagonal wurtzite structure with lattice parameters of a = b = 0.325 nm and c = 0.521 nm. Because of all these characteristics, they are used extensively in a variety of applications, including photovoltaic applications, solar cells, light-emitting diodes, and photocatalysis(Lhimr et al., 2021). The fact that ZnO films contain components that are abundant in soil and do not face the risk of depletion gives them a significant advantage over ITO (Gultepe & Atay, 2022).

Transparent conductive oxide (TCO) thin films have become more efficient as a result of the development of low-cost, high-performance optoelectronic devices. These technologies have significant applications in the fields of solar cells, liquid crystal displays, heat mirrors, gas sensors, optical position sensors, photothermal conversion systems, and acoustic wave transducers (Chavan et al., 2023). Zinc oxide (ZnO) has been one of the most promising TCO materials in recent years due to its natural availability, strong chemical and mechanical resilience, and good optical and electrical qualities. This reduces the material's cost in comparison to the most popular TCO materials (ITO, SnO2)(Naser et al., 2022). For figuring out the physical characteristics and uses of different materials, particularly semiconductors, doping is essential. Exceptionally successful applications in the semiconductor industry have validated this idea. The carrier concentrations and electrical conductivities of the materials are determined by minute amounts of impurities. Essentially, a good dopant should have a shallow defect level and reach optimal solubility in its host material(Zhang et al., 2016). ZnO is doped by adding higher valence atoms from metals like gallium, indium, and aluminum in place of Zn2+ atoms. The effectiveness is determined by the electronegativity of the dopant element and the ionic radius difference of zinc (Potter et al., 2018). Owing to its elevated electrical resistance, ZnO exhibits worse competitiveness in comparison to ITO and has restricted use in photovoltaic solar cells. The conductivity and transparency of ZnO films have been significantly enhanced by IIIA, IIIB, IVA, and IVB cations or non-metal anions(Gultepe & Atay, 2022). One of the most effective ways to increase the electrical conductivity and potential use of pure-ZnO films in PV applications is to adopt the co-incorporating technique. Compared to single-cation doping, ZnO sample resistivity decreases more with both forms of co-doping. Co-doping with metals including copper (Cu), manganese (Mn), cobalt (Co), and titanium (Ti) has been shown in several studies to improve the material's electrical and optical properties by controlling the Zn vacancies in the ZnO crystal structure(Jang et al., 2023). It has been shown that Al-doped ZnO exhibits increased optical and electrical conductivity, which makes it advantageous for use in transparent conductive electrodes and solar cells, among other applications(Badgujar et al., 2022). Typically, a B-doping result in an increase in carrier density, which boosts the tunneling current in n-type semiconductors. The element boron has the highest electro negativity and the lowest ionic radius (0.23 Å). Furthermore, B^{3+} has a noticeably stronger Lewis acid (10.7) than Al^{3+} (3.04). Consequently, ZnO nanostructures physical characteristics may be effectively adjusted using boron doping(Pandey et al., 2017). The Al-B co-doping strategy significantly improves the optical, surface, and electrical properties of ZnO film as compared to simply the Al-incorporating process, which makes it highly suitable for TCO applications. The resistivity of ZnO film decreased from 6.12×102 Ωcm to $2.07 \times 10–4$ Ωcm following Al–B co-doping treatment. Furthermore, the presence of Al and B components led to a considerable increase in the ZnO film's transmittance values, surface homogeneity, and figure of merit value. All of the research has demonstrated that Al–B co-incorporated ZnO films are a good alternative to ITO films in TCO applications because to their favorable physical characteristics. But when compared to ITO, the preferred material for photovoltaic solar cell applications, the electrical conductivity of AZO and BZO samples created via the sol-gel method is still poor(Gultepe & Atay, 2022). By using the same amount of precursor concentration for both Al and B while maintaining a constant ZnO precursor concentration, the research aims to improve the window layer of the solar cell's current transmittance and carrier mobility. The sol-gel approach will be used in this work to generate undoped and Co-doped ZnO thin films on glass substrates using the dip-coating technique. In order to maximize the efficiency of solar cell collectors, the structural characteristics of the thin films will be examined.

MATERIALS AND METHODS

3g of Zinc acetate dihydrate ($Zn(CH_3CO_2)_2.2H_2O$) was dissolved in 50 ml of 2-methoxyethanol ($(CH_3)_2CHOH$, Aldrich, 99.8%), and rapidly agitated with a magnetic stirrer at room temperature for 15 minutes according to (Bouacheria et al., 2022). As a stabilizer, monoethanolamine (MEA: $H_2NCH_2CH_2OH$, Aldrich, 99.5%,) was added drop-wise while stirring continuously at a molar ratio of 1:1 in the MEA mixture as adopted by Saleem *et al*., (2012). After an hour of stirring at 60˚C, the resulting solution became clear and uniform, ready for coating. To guarantee that a homogenous, transparent solution is produced, the resultant mixture was further agitated for 40 minutes. After that, the mixture was centrifuged at 3500 rpm to get rid of the unreacted components. (Musleh *et al*.,

2018) and then filtrated by using the standard 0.45µm filter paper as adopted by(Alsaad et al., 2020). The next stage was the Preparation of Al – doped ZnO (A:ZnO) and B- doped ZnO (B:ZnO) Solutions The process involved incorporating 2g of boric acid (H_3BO_3) into the ZnO solution to create B:ZnO and 2g of aluminum nitrate ($Al(NO_3)_3 9H_2O$) into the ZnO solution to create A:ZnO accordingly. Using a magnetic stirrer for two hours at 60 ^OC, a transparent solution for each of the doped systems was created. Lastly, 0.45µm filter paper was used to filter the resultant solution. At room temperature, the corresponding solution was swirled for two hours at 60 ^OC. To allow for aging, the colorless, transparent, homogenous solution was left at room temperature for 24 hours respectively. This procedure was followed strictly to ensure the creation of solutions that can maintain a high degree of transparency. To prepare the A: B: ZnO both solutions were combined. For hydrolysis and condensation, the corresponding solution was stirred for two hours at room temperature at 60 ^OC. To allow for the aging process, the colorless, transparent, homogenous solution was being kept at room temperature for a full day. Following the preparation of the solutions with the required characteristics, the glass substrate was dipped in the sol and removed using the dip-coating process at the rate of 0.9cm/min in room temperature for three hours.This method enabled the production of thin films with an average thickness of 300 nm. After that, the produced films were dried in an oven for 15-20 minutes at 200 to 300 ^OC in order to remove the solvent and any polluted organic residues. For the organics to completely evaporate and for the ZnO film to begin forming and crystallizing, the temperature of the preheat treatment is very necessary. This process was followed by annealing in air at a temperature of 500 ^OC for three hours(Stroescu et al., 2023).

RESULTS AND DISCUSSION

XRD of ZnO, ZnO/Al, ZnO/B and ZnO/Al/B

One of the method most frequently used to characterize nanoparticles NPs is X-ray diffraction (XRD). XRD typically yields data on the crystalline grain size, lattice parameters, phase nature, and crystalline structure. The lattice parameter is determined for a given sample using the Scherrer equation and the broadening of the measurement's most intense peak from XRD analysis (Tatjana et al., 2022). The position and strength of the peaks can be compared to reference patterns obtained from the database of the International Centre for Diffraction Data (ICDD, formerly known as the Joint Committee on Powder Diffraction Standards, JCPDS) to ascertain the composition of the particles (Mourdikoudis et al., 2018). The XRD patterns of ZnO, ZnO:Al, ZnO:B, and ZnO:Al:B as shown in Fig. 1 were carried out to investigate their crystalline structures, phase composition, crystallite size, and the effects of doping with aluminum (Al), boron (B), and a combination of Al and B. The XRD pattern of ZnO shows several distinct peaks, which correspond to the crystalline planes of ZnO in a hexagonal wurtzite structure, in line with the JCPDS card No. 36-1451. The prominent peaks are located at 2θ values of approximately 31.7°, 34.4°, 36.2°, 47.5°, 56.6°, 62.8°, and 67.9°. These peaks correspond to the (100), (002), (101), (102), (110), (103), and (112) planes, respectively. The sharpness and intensity of these peaks indicate that the ZnO nanoparticles are highly crystalline. Furhan and Ramesan (2022) reported similar diffraction peaks, corresponding to the same crystal planes. This alignment with the indexed planes confirms the structural integrity and crystallinity of the synthesized ZnO nanoparticles. Additionally, Bahtoun *et al*. (2023) emphasized that the sharpness and intensity of these peaks are crucial indicators of high crystallinity, which is essential for applications such as photocatalysis and optoelectronics.

The lattice spacing of undoped ZnO, Al doped ZnO and B doped ZnO thin films were calculated using the Bragg's formula (Saliha, 2010).

$$2d_{hkl} \sin\theta = n\lambda \quad (1)$$

Where (h k l) are Miller indices; dhkl is the lattice spacing; θ is half of Bragg angle; and λ is the wavelength of the target XRD. Further, the lattice parameters (a,c) values calculated from the spectra obtained, determined from relation (Bouacheria et al., 2022).

$$\frac{1}{d_{hkL}^2} = \frac{h^2 + k^2}{a^2} + \frac{1}{c^2} \quad (2)$$

The Debye-Scherrer formula as expressed in Equ. 4 is employed to estimate the crystallite size from the XRD peak broadening. The crystallite size is 20.4 nm, confirming the nanoscale nature of the synthesized particles.

$$D = \frac{k\lambda}{\beta\cos\theta} \quad (3)$$

where D is the crystallite size (nm), k is a constant (0.94 for spherical particles), λ is the wavelength of the X-ray radiation (CuKaα = 0.1541 nm), β is the full width at half maximum (FWHM) of the XRD peak (in radians) and θ is the Bragg's or diffraction angle (in degree) (Bouacheria et al., 2022).

Using the Scherrer formula of equation 3

Average crystallite size: 20.4 nm

Lattice parameters: a ≈ 0.325 nm, c ≈ 0.521 nm

Aspect ratio: c/a ≈ 1.6

The estimated crystallite size agrees with the diameters of the ZnO nanoparticles. Lattice characteristics match the wurtzite structure of ZnO, XRD examination confirmed that ZnO has a hexagonal structure. A

crystalline size of 20.4 nm is suitable for solar cells' window layer (Amjad et al., 2022). The XRD pattern of ZnO/Al, which represents ZnO doped with aluminum, is presented in Fig. 1(c). While the pattern remains similar to that of pure ZnO, there are noticeable changes. There is a slight shift in the 2θ values of the peaks to higher angles, especially for the (101) and (002) planes. This shift suggests a contraction of the unit cell as a result of Al doping. The observed shift is consistent with Vegard's law, which states that the substitution of smaller ions in a host lattice leads to a decrease in lattice parameters. Ijaz (2024). demonstrated that in Al-doped hexaferrites, the lattice parameters 'a' and 'c' decreased with increasing Al content, aligning with the expectations set by Vegard's law. Similarly, Ashour *et al*. (2022) investigated Al-doped zinc oxide thin films and reported a contraction in the crystalline structure as the Al doping concentration increased, further validating the assertion that smaller ions lead to reduced lattice dimensions. The intensity of the diffraction peaks decreases, indicating a reduction in crystallinity upon Al doping (Ashour *et al.*, 2022). This phenomenon can be attributed to the substitution of Zn^{2+} ions by Al^{3+} ions, which introduces lattice distortions due to the smaller ionic radius of Al^{3+} (0.54 Å) compared to Zn^{2+} (0.74 Å). This substitution creates strain in the ZnO lattice, which affects the crystallite size and peak broadening. The crystallite size (31.4 nm) calculated for ZnO:Al is larger than that of pure ZnO (Urakawa, 2024).

The XRD pattern of ZnO:B, representing ZnO doped with boron shown in Fig.1 b, indicate a more significant reduction in peak intensity compared to both pure ZnO and ZnO:Al. This observation indicates a more pronounced reduction in crystallinity, which could be due to the larger ionic radius of B^{3+} (0.58 Å) compared to Al^{3+}, though still smaller than Zn^{2+}. Boron doping introduces greater disorder into the ZnO lattice, leading to lattice distortions and defects. There is a noticeable shift in the peak positions toward lower 2θ values, especially in the (101), (002), and (100) planes. This shift is indicative of an expansion of the unit cell, which can be attributed to the incorporation of B^{3+} ions. This is corroborated by studies that report similar shifts in diffraction peaks with the introduction of various dopants, including boron, which alters the lattice parameters of ZnO (Özel and Atilgan, 2023; Al-Qadasy, 2024; Oeba and Mosiori, 2022). The substitution of Zn^{2+} by B^{3+} creates oxygen vacancies and lattice strain, resulting in peak broadening. The degree of broadening is more significant in ZnO:B compared to ZnO:Al, indicating that B doping induces greater disorder in the ZnO structure. The crystallite size (22.6 nm) for ZnO:B is also reduced compared to ZnO:A. This reduction in crystallite size, coupled with the increase in surface defects, can improve the photocatalytic properties of ZnO:B by providing more active sites for catalytic reactions.

The XRD pattern of ZnO:Al:B, which represents ZnO co-doped with aluminum and boron, shows a combination of the effects observed in ZnO:Al and ZnO:B (Fig. 1d). The diffraction peaks exhibit significant broadening and reduced intensity, indicating a substantial reduction in crystallinity. The XRD pattern also confirms that the reduced grain size value is a sign of the damaged crystal structure. The deteriorating crystal structure is shown by the decreasing grain size value, which the XRD pattern also confirms. By decreasing ZnO diffusion, Al^{3+} ions create a retarding force that prevents ZnO from forming at the grain boundary surface defects and smaller ion radius of element B. We believe that this may be the cause of this(Gultepe & Atay, 2022). The peak positions show a slight shift to higher 2θ values compared to pure ZnO, similar to ZnO:Al, but the broadening is more pronounced due to the combined effects of Al and B doping. The shift in 2θ values suggests that the co-doping of Al and B leads to a complex interplay between lattice contraction and expansion. The smaller Al^{3+} ions reduce the lattice parameters, while the larger B^{3+} ions tend to expand the lattice. The overall effect is a slight contraction, as evidenced by the shift toward higher angles, but the increased peak broadening indicates that co-doping introduces significant lattice strain and defects. The effect of larger ions, such as B^{3+}, on lattice expansion is evident in studies of Khoreem (2023), which noted that the substitution of lower ionic radius ions with larger ions results in an increase in lattice parameters. This is consistent with the findings of (Hunize et al., 2022), who observed that the introduction of Nd^{3+} ions, which have a larger ionic radius compared to the ions they replace, leads to an increase in lattice dimensions.

TABLE 1: Lattice Parameters

NANOPARTICLES	LATTICE PARAMETERS(CONSTANT)	AVERAGE CRYSTALINE SIZE
ZNO	a ≈ 3.25 Å b ≈ 3.25 Å c ≈ 5.21 Å	20.4nm
ZNO:A	a ≈ 3.25Å b ≈ 3.25 Å c ≈ 5.21 Å	31.4nm
ZNO:B	a ≈ 3.21Å b ≈ 3.21 Å c ≈ 4.844Å	22.6 nm
ZNO:A:B	a ≈ 3.21Å b ≈ 3.21 Å c ≈ 4.844Å	16.7 nm

The ZnO co-doped with Al and B has substantial advantages for use as a window layer in solar cells according to the results of the XRD study. The co-doped ZnO sample's contracted crystal lattice and smaller crystallite size (16.7 nm) may result in increased conductivity and transparency, two qualities necessary for a window layer in solar cells (Ellmer, 2000). Lattice contraction and decreased crystallite size can also lead to increased carrier mobility, which is essential for effective charge transfer in solar cells (Kim et al., 2013). According to Lee et al. (2014), the co-doped ZnO's reduced crystallite size and changed lattice characteristics may result in higher UV-Vis transmittance, which would let more sunlight into the absorber layer and boost the solar cell's overall efficiency.

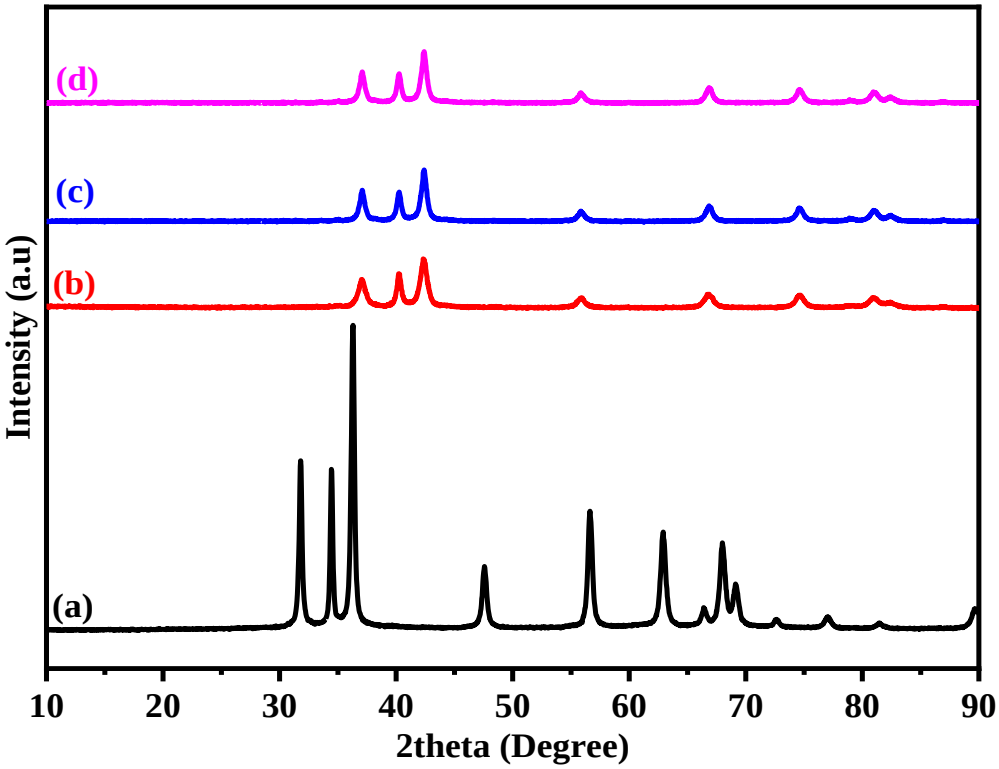

Figure 1: XRD patterns of (a) ZnO (b) ZnO:Al (c) ZnO:B (d) ZnO:Al:B

High- resolution Scanning Electron Microscope and Energy- Dispersive X-ray Spectroscopy (HRSEM/EDX) of ZnO, ZnO:Al, ZnO:B and ZnO:Al:B

The HRSEM images of the synthesized ZnO, ZnO:Al, ZnO:B, and ZnO:Al:B samples as presented in Fig.2 give information about the morphological features and surface characteristics of these materials. The HRSEM image of pure ZnO nanoparticles shows a predominantly spherical morphology, which is consistent with the well-documented crystal growth patterns of ZnO (Fig. 2(a). The spherical particles tend to cluster together, forming aggregated structures, likely due to the high surface energy of ZnO, which drives particle interaction and agglomeration. The average particle size of the synthesized ZnO nanoparticles is 32.17 nm. The spherical nature of ZnO observed in the HRSEM images indicates a high surface-to-volume ratio, a desirable feature for photovoltaic applications (Shaba *et al.,* 2023). Moreover, the absence of any significant defects in the surface morphology suggests that the ZnO synthesis process was successful, yielding high-quality nanoparticles.

Incorporating aluminum (Al) into ZnO leads to significant morphological changes, as evidenced by the HRSEM images of ZnO:Al nanoparticles shown in Fig. 2(b). The ZnO:Al nanopaticles shows a more spherical particles-like structure, indicating that Al doping alters the nucleation and growth patterns of ZnO during synthesis. The presence of Al modifies the surface energy of ZnO, facilitating anisotropic growth along specific crystal facets, resulting in the formation of more spherical shape particles. The structure offers an increased aspect ratio, which can enhance the material's surface reactivity in applications like window layers of solar cells. This aligns with the assertion that Al modifies the surface energy, which in turn affects the anisotropic growth of ZnO (Sugihartono *et al.,* 2023). Furthermore, Zhao *et al.* (2023) demonstrate that Al decoration on ZnO nanoflower matrices enhances their gas sensing properties, suggesting that the structural modifications imparted by Al doping can lead to improved surface reactivity, a crucial factor in photocatalytic applications. Furthermore, the HRSEM images reveal a reduction in the degree of agglomeration compared to pure ZnO. This is likely due to the presence of Al, which may hinder the strong van der Waals forces that typically lead to nanoparticle agglomeration, thereby promoting a more dispersed morphology.

When boron (B) is introduced into the ZnO lattice, the HRSEM images reveal a further shift in morphology compared to pure ZnO and ZnO:Al (see Fig. 2c). The ZnO:B nanoparticles exhibit a mixed morphology of both spherical and sheet-like structures. The spherical particles are similar in size to those observed in pure ZnO, but the presence of B induces the formation of nanoparticles, which suggests that B alters the crystal growth mechanisms during synthesis. The nanoparticles structure could be the result of boron doping, which is known to promote layered growth, inhibiting crystal growth along specific crystallographic planes. The HRSEM images also show less aggregation in ZnO:B than in pure ZnO, which could be attributed to the influence of boron on particle. The incorporation of boron has been linked to the formation of B—O bonds, which contribute to the distinct vibrational modes observed in the doped ZnO, further supporting the claim that boron influences the structural characteristics of these nanoparticles (Khalid *et al.,* 2022).

The HRSEM images of ZnO:Al:B nanoparticles display the most complex morphology among the synthesized materials, reflecting the combined influence of both Al and B doping. The ZnO:Al:B sample exhibits a mixture of spherical particles. The spherical particles resemble those observed in pure ZnO, while the smaller particles are similar to those seen in ZnO:Al, and ZnO:B.

The hierarchical structure of ZnO:Al:B suggests that the simultaneous incorporation of Al and B creates a synergistic effect on the crystal growth and morphology of ZnO as shown in Fig 2(d). The presence of Al appears to promote anisotropic growth, leading to spherical-like structures, while B induces the formation of more spherical-like particles, resulting in hybrid morphology. The HRSEM image reveals that the ZnO/Al/B nanoparticles exhibit the least amount of particle agglomeration among the samples. This reduced agglomeration can be attributed to the combined effects of Al and B, which likely modify the surface chemistry of ZnO in a way that prevents strong particle interactions. The work of Al-Farsi et al. (2022) demonstrated that Al-doped ZnO nanorods exhibit altered optical properties and enhanced surface area, which can contribute to reduced agglomeration by minimizing particle interactions through improved surface passivation. The well-dispersed particles and the complex morphology of ZnO:Al:B suggest that this material could have superior optoelectronics properties compared to pure ZnO.

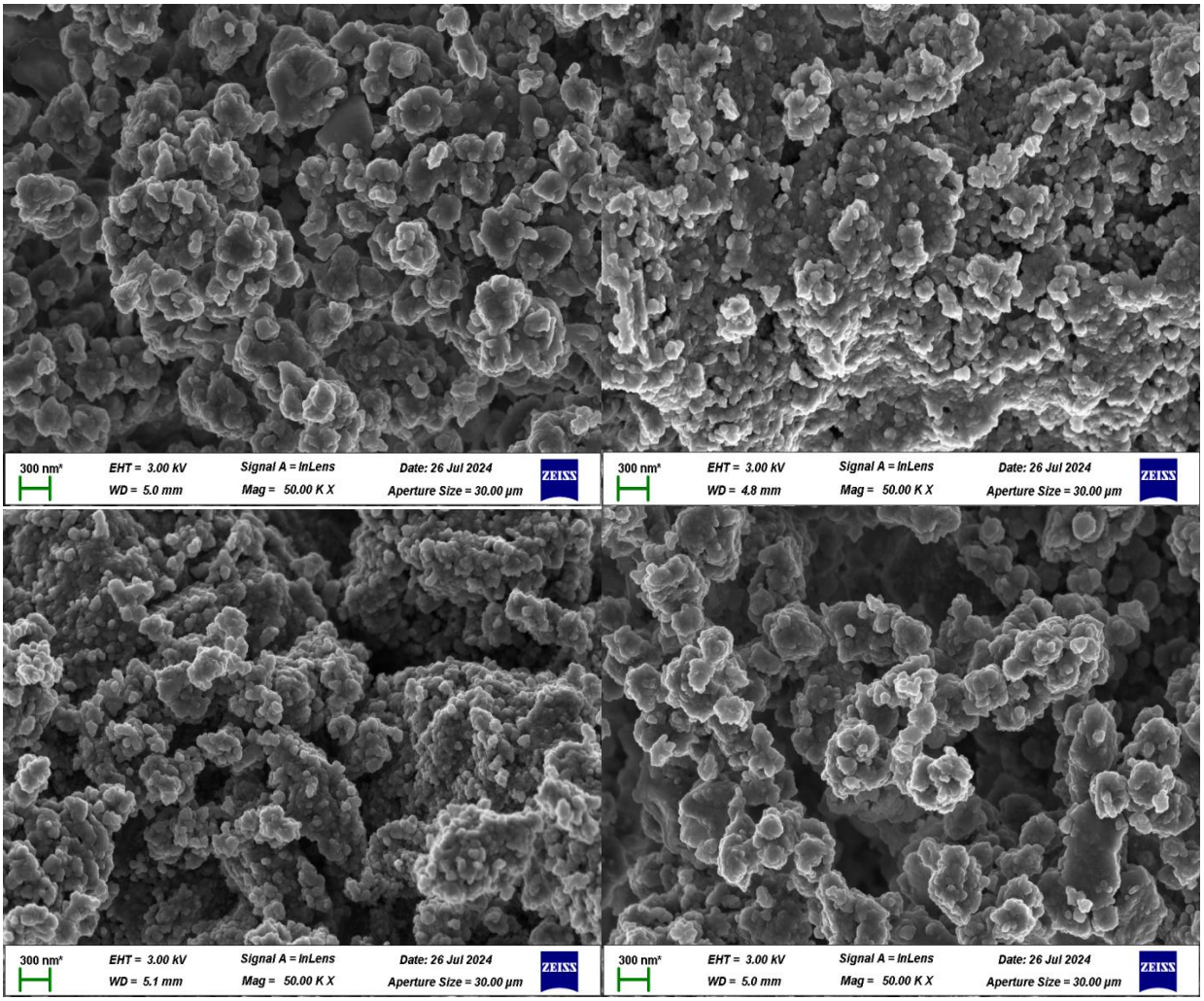

Figure 2: HRSEM images of (a) ZnO (b) ZnO:Al (c) ZnO:B (d) ZnO:Al:B

The elemental compositions of ZnO, ZnO:Al, ZnO:B, and ZnO:Al:B as presented in Fig. 3 were analyzed using EDX, revealing the doping of aluminum (Al) and boron (B) into ZnO. The EDX spectra of the ZnO sample revealed the presence of two major elements: zinc (Zn) and oxygen (O) (Fig. 3a). In this case, Zn was found to be the dominant element, constituting a significant portion of the composition, while oxygen was present in stoichiometric proportions relative to Zn. The observed Zn ratio closely matches the expected stoichiometry of ZnO, which is 1:1. The elemental analysis confirms the successful synthesis of pure ZnO without any significant impurities. The absence of other elements in the EDX spectrum further supports the high purity of the synthesized ZnO, making it a suitable candidate for comparison with doped materials.

In the EDX spectrum of ZnO:Al (Fig. 3b), in addition to the Zn and O peaks, a distinct peak corresponding to Al was observed, confirming the successful incorporation of Al into the ZnO lattice. The presence of Al in ZnO:Al is significant as it suggests that Al has been successfully doped into the ZnO structure, potentially substituting for Zn in the crystal lattice due to the similar ionic radii of Al^{3+} (0.54 Å) and Zn^{2+} (0.74 Å) (Raship *et al.*, 2022; Ashour *et al.*, 2022). The atomic percentage of Al in the ZnO:Al sample was relatively low, indicating that Al was present as a dopant rather than as a major constituent. This is expected, as doping typically involves the introduction of small quantities of foreign atoms to modify the host material's properties. The ratio of Zn to O in the doped sample remained close to 1:1, suggesting that the doping process did not significantly disrupt the stoichiometry of the ZnO lattice. The presence of Al could introduce additional defect sites and oxygen vacancies in the ZnO structure, which could enhance photocatalytic performance by promoting charge separation and increasing the number of active sites for redox reactions. Furthermore, Al doping could also lead to a reduction in the bandgap energy, improving the material's ability to absorb visible light.

The EDX spectrum of ZnO:B revealed the successful incorporation of boron into the ZnO matrix, as evidenced by the presence of a distinct B peak alongside the Zn and O peaks (Fig. 3c). The atomic percentage of B in the doped sample was also relatively low, consistent with the expected behaviour of B as a dopant. Boron atoms are much smaller than Zn atoms, with an ionic radius of B^{3+} (0.23 Å) significantly smaller than that of Zn^{2+}. This difference in size suggests that B is more likely to occupy interstitial sites in the ZnO lattice rather than substituting directly for Zn. As a result, B doping could introduce structural distortions and create oxygen vacancies, which could influence the material's properties significantly (Yüksel et al., 2022; Üzar, 2024).

The ZnO:Al:B sample represents a dual-doped system, where both Al and B have been incorporated into the ZnO lattice. The EDX spectrum of ZnO:Al:B sample showed the presence of peaks corresponding to Zn, O, Al, and B, confirming the successful co-doping of Al and B into the ZnO structure. The atomic percentages of Al and B were both relatively low, consistent with their roles as dopants. The co-doping of Al and B is expected to introduce a synergistic effect, where the individual benefits of Al and B doping are combined to enhance the material's overall performance. The Zn ratio in the ZnO:Al:B sample was similar to that of the other samples, indicating that the co-doping process did not significantly disrupt the stoichiometry of the ZnO lattice. However, the presence of both Al and B is expected to introduce more defect sites and oxygen vacancies than single-doped systems, potentially leading to improved photocatalytic properties.

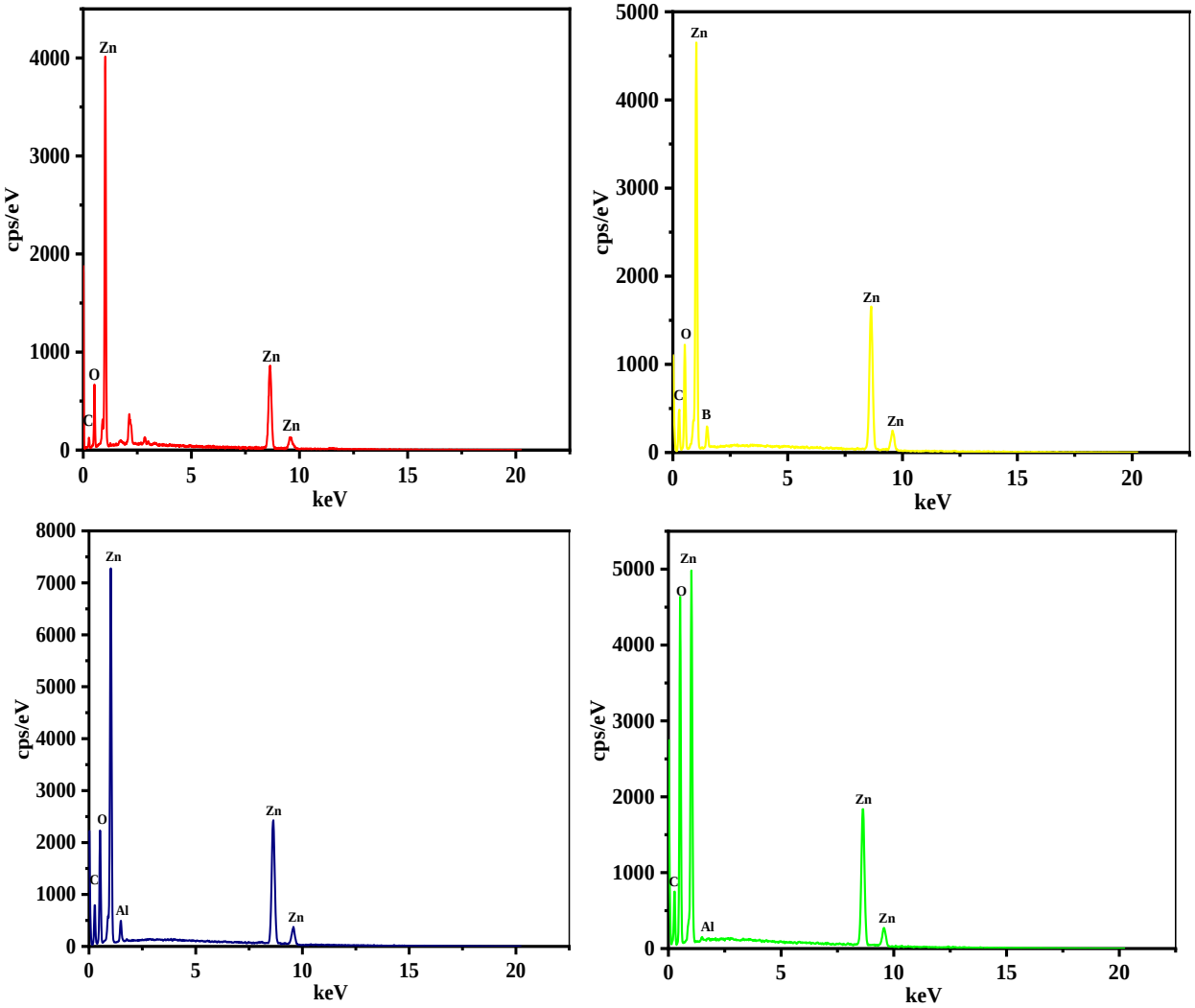

Figure 3: EDX spectra of (a) ZnO (b) ZnO:Al (c) ZnO:B (d) ZnO:A:B

CONCLUSION

In conclusion, this research demonstrates the significant impact of Al and B doping on the structural properties of ZnO nanoparticles synthesized via the sol-gel method. HRSEM analysis reveals distinct morphological changes, including variations in particle shape, size, and agglomeration, upon incorporation of Al and B. The simultaneous doping of Al and B in ZnO:Al:B nanoparticles creates a synergistic effect, resulting in a complex hierarchical structure with reduced particle agglomeration. These structural modifications are expected to enhance the surface reactivity and optoelectronic properties of ZnO, making ZnO:Al:B a promising material for window layers in solar cells. The findings of this study contribute to the optimization of ZnO-based nanostructures for photovoltaic applications and provide a foundation for further investigation into the effects of doping on ZnO's electronic and optical properties. Further research can be carried by varying the precursor concentration of Al and B for better efficiency of window layer of solar cells.

REFERENCE

Al-Farsi, L., Souier, T. M., Al-Hinai, M., Myint, M. T., Kyaw, H. H., Widatallah, H. M., & Al- Abri, M. (2022). pH Controlled Nanostructure and Optical Properties of ZnO and Al- doped ZnO nanorod arrays grown by microwave-assisted hydrothermal method. *Nanomaterials*, *12*(21), 3735.

Al-Qadasy, S. (2024). Effect of boron-doping and annealing on the structure, morphological and optical properties of zno films prepared by spray pyrolysis method. Physica Scripta, 99(6), 0659a3.

Alsaad, A. M., Ahmad, A. A., Qattan, I. A., Al-Bataineh, Q. M., & Albataineh, Z. (2020). Structural, optoelectrical, linear, and nonlinear optical characterizations of dip-synthesized undoped zno and group iii elements (B, al, ga, and in)-doped zno thin films. *Crystals*, *10*(4). https://doi.org/10.3390/cryst10040252

Amjad, M., Khan, M. I., Alwadai, N., Irfan, M., Ikram-Ul-haq, Albalawi, H., Almuqrin, A. H., Almoneef, M. M., & Iqbal, M. (2022). Photovoltaic Properties of ZnO Films Co-Doped with Mn and La to Enhance Solar Cell Efficiency. *Nanomaterials*, *12*(7). https://doi.org/10.3390/nano12071057

Ashour, A., Assem, E., & Shaaban, E. (2022). Investigation of dilute aluminum doped zinc oxide thin films: structural and morphological properties for varies applicationss. Journal of Ovonic Research, 18(5), 699-711.

Badgujar, A. C., Yadav, B. S., Jha, G. K., & Dhage, S. R. (2022). Room Temperature Sputtered Aluminum-Doped ZnO Thin Film Transparent Electrode for Application in Solar Cells and for Low-Band-Gap Optoelectronic Devices. *ACS Omega*, *7*(16), 14203–14210. https://doi.org/10.1021/acsomega.2c00830

Bahtoun, H., Hadjeris, L., Iaiche, S., & Ounis, T. (2023). Effect of zno nanoparticles salt precursors on structural, morphological, optical and mb photocatalytic properties using hydrothermal synthesis. Journal of Nano Research, 77, 87-104.

Bouacheria, M. A., Djelloul, A., Adnane, M., Larbah, Y., & Benharrat, L. (2022). Characteristics of ZnO and Al Doped ZnO Thin Films Prepared by Sol Gel Method for Solar Cell Applications. *Journal of Inorganic and Organometallic Polymers and Materials*, *32*(7), 2737–2747. https://doi.org/10.1007/s10904-022-02313-0

Chavan, G. T., Kim, Y., Khokhar, M. Q., Hussain, S. Q., Cho, E. C., Yi, J., Ahmad, Z., Rosaiah, P., & Jeon, C. W. (2023). A Brief Review of Transparent Conducting Oxides (TCO): The Influence of Different Deposition Techniques on the Efficiency of Solar Cells. *Nanomaterials*, *13*(7). https://doi.org/10.3390/nano13071226

Ellmer, K. (2000). Resistivity of polycrystalline ZnO films: current status and physical limit. Journal of Physics D: Applied Physics, 33(4), R17-R32.

Furhan, & Ramesan, M. T. (2022). Enhanced dielectric properties, thermal stability and ammonia sensing performance of poly (diphenylamine)/zinc oxide nanocomposites via one step polymerization. *Journal of Applied Polymer Science*, *139*(38), e52913.

Gultepe, O., & Atay, F. (2022). Al and B co-doped ZnO samples as an alternative to ITO for transparent electronics applications. *Journal of Materials Science: Materials in Electronics*, *33*(18), 15039–15053. https://doi.org/10.1007/s10854-022-08421-4

Hunize, C., Joseph, M., & Murali, K. (2022). Synthesis and dielectric characterization of nd doped srtio₃ ceramics for energy storage applications. Key Engineering Materials, 928, 113- Jang, S., Karade, V. C., Jang, J. S., Jo, E., Shim,

H., Kim, S. G., Patil, K., Gour, K. S., & Kim, J. H. (2023). Achieving over 10% device efficiency in Cu2ZnSn(S,Se)4 thin-film solar cells with modifications of window layer properties. *Journal of Alloys and Compounds*, *930*, 167302.

https://doi.org/10.1016/j.jallcom.2022.167302

Ibrahim, N. B., Al-Shomar, S. M., & Ahmad, S. H. (2013). Effect of annealing temperature on the structural and optical properties of nanocrystalline ZnO thin films prepared by sol-gel method. *Sains Malaysiana*, *42*(12), 1781–1786.

Ijaz, M. (2024). Microstructural, morphological and magnetic behaviour of al3+ replaced bafe11.5co0.5o19 hexaferrites synthesized via sol-gel auto combustion route. Physica Scripta, 99(5), 055959

Jang, S., Karade, V. C., Jang, J. S., Jo, E., Shim, H., Kim, S. G., Patil, K., Gour, K. S., & Kim, J. H. (2023). Achieving over 10% device efficiency in Cu2ZnSn(S,Se)4 thin-film solar cells with modifications of window layer properties. *Journal of Alloys and Compounds*, *930*, 167302. https://doi.org/10.1016/j.jallcom.2022.167302

Khalid, A., Ahmad, P., Muhammad, S., Khan, A., Khandaker, M.U., Alam, M.M., Asim, M., Din, I.U., Iqbal, J., Rehman, I.U. and Razzaq, Z., 2022. Synthesis of boron-doped zinc oxide nanosheets by using phyllanthus emblica leaf extract: a sustainable environmental application. *Frontiers in Chemistry*, *10*, p.930620.

Khan, Z. R., Khan, M. S., Zulfequar, M., & Shahid Khan, M. (2011). Optical and Structural Properties of ZnO Thin Films Fabricated by Sol-Gel Method. *Materials Sciences and Applications*, *02*(05), 340–345. https://doi.org/10.4236/msa.2011.25044

Khantoul, A. R., Sebais, M., Rahal, B., Boudine, B., & Halimi, O. (2018). Structural and optical properties of zno and co doped ZnO thin films prepared by sol-gel. *Acta Physica Polonica A*, *133*(1), 114–117. https://doi.org/10.12693/APhysPolA.133.114

Khoreem, S. (2023). Effect of nonmagnetic doping on dielectric properties and initial permeability of ba-ni ferrite nanoparticles by virtue of Zn^{2+} ions. Advances in Materials Science and Engineering, 2023, 1-10.

Kim, H., Kim, D., Kim, Y., Lee, S., & Lee, J. (2013). Effects of Al doping on the electrical and optical properties of ZnO thin films. Journal of Alloys and Compounds, 574, 532-536.

Lee, J., Lee, S., Kim, H., Kim, D., & Kim, Y. (2014). Enhanced UV-Vis transmittance and electrical conductivity of ZnO:Al thin films by B doping. Journal of Materials Science: Materials in Electronics, 25(10), 4336-4342.

Lhimr, S., Bouhlassa, S., & Ammary, B. (2021). Influence of calcination temperature on size, morphology and optical properties of zno/c composite synthesized by a colloidal method. *Indonesian Journal of Chemistry*, *21*(3), 537–545. https://doi.org/10.22146/ijc.56309

Mourdikoudis, S., Pallares, R. M., & Thanh, N. T. K. (2018). Characterization techniques for nanoparticles: Comparison and complementarity upon studying nanoparticle properties. *Nanoscale*, *10*(27), 12871–12934. https://doi.org/10.1039/c8nr02278j

Musleh, H., AlDahoudi, N., Zayed, H., Shaat, S., Tamous, H. M., Shurrab, N., Issa, A., & Asad, J. (2018). Synthesis and Characterization of Zno Nanoparticles Using Hydrothermal and Sol-Gel Techniques for Dye-Sensitized Solar Cells. *Journal of University of Babylon for Engineering Sciences*, *26*(9), 256–267. https://doi.org/10.29196/jubes.v26i9.1736

Naser, A., Hachim, D., & Abed, Q. (2022). *A review of Effect the Zinc Oxide deposition on Crystalline Silicon Solar Cells.* https://doi.org/10.4108/eai.7-9-2021.2314810

Oeba, D. and Mosiori, C. (2022). Electrical and optical properties of boron doped zinc oxide thin-film deposited by metal-organic chemical vapour deposition for photovoltaic application. Physical Science International Journal, 48-55.

Özel, K. and Atilgan, A. (2023). Systematic investigation on the synergistic impact of gallium (ga)-boron (b) co-doping on the features of zno films. Gazi University Journal of Science Part A: Engineering and Innovation, 10(4), 442-451.

Pandey, V., Singh, N., & Haque, F. Z. (2017). Enhancement in Structural and Optical Properties of Boron Doped ZnO Nanostructures Synthesized by Simple Aqueous Solution Growth Technique. *Journal of Advanced Physics*, *6*(3), 358–366. https://doi.org/10.1166/jap.2017.1333

Potter, D. B., Powell, M. J., Parkin, I. P., & Carmalt, C. J. (2018). Aluminium/gallium, indium/gallium, and aluminium/indium co-doped ZnO thin films deposited: Via aerosol assisted CVD. *Journal of Materials Chemistry C*, *6*(3), 588–597. https://doi.org/10.1039/c7tc04003b

Raship, N. A., Tawil, S. N. M., Nayan, N., Ismail, K., Bakri, A. S., & Mohkhter, F. (2022). Investigation on the structural and electrical properties of zno thin films

co-doped with rare earth gd and al prepared by co-sputtering method. Materials Science Forum, 1053, 143-147.

Regmi, G., Rijal, S., & Velumani, S. (2023). Aluminum-doped zinc oxide (AZO) ultra-thin films deposited by radio frequency sputtering for flexible Cu (In , Ga) Se 2 solar cells. *Memories - Materials, Devices, Circuits and Systems*, *5*(June), 100064. https://doi.org/10.1016/j.memori.2023.100064

Saleem, M., Fang, L., Wakeel, A., Rashad, M., & Kong, C. Y. (2012). Simple Preparation and Characterization of Nano-Crystalline Zinc Oxide Thin Films by Sol-Gel Method on Glass Substrate. *World Journal of Condensed Matter Physics*, *02*(01), 10–15. https://doi.org/10.4236/wjcmp.2012.21002

Saliha I., Mujdat C. and Yasemin C. (2010) Sn doping effects on the electro-optical properties of sol gel derived transparent ZnO films, Applied Surface Science, Volume 256(23), 7204-7210, ISSN 0169-4332

Shaba, E. Y., Tijani, J. O., Jacob, J. O., & Suleiman, M. A. T. (2023). Effect of mixing ratios of SiO2 nanoparticles synthesized from metakaolin on the physicochemical properties of ZnO/SiO2 nanocomposites. *Nano-Structures & Nano-Objects*, *35*, 101003.

Speaks, D. T. (2020). Effect of concentration, aging, and annealing on sol gel ZnO and Al-doped ZnO thin films. *International Journal of Mechanical and Materials Engineering*, *15*(1). https://doi.org/10.1186/s40712-019-0113-6

Stroescu, H., Nicolescu, M., Mitrea, D., Tenea, E., Atkinson, I., Anastasescu, M., Calderon-Moreno, J. M., & Gartner, M. (2023). Effect of Al Incorporation on the Structural and Optical Properties of Sol–Gel AZO Thin Films. *Materials*, *16*(9). https://doi.org/10.3390/ma16093329

Sugihartono, I., Tan, S.T., Arkundato, A., Fahdiran, R., Isnaeni, I., Handoko, E., Budi, S. and Budi, A.S., 2023. The Effect of Al-Cu Co-Dopants on Morphology, Structure, and Optical Properties of ZnO Nanostructures. *Materials Research*, *26*, p.e20220499.

Tatjana S., Konstantinos K., andJohn D. K (2022) Box-Behnken design to optimise 3D printing parameters in applications for fashion products, International Journal of Experimental Design and Process Optimisation 7(1):49-61

Urakawa, S. (2024). Sputter deposition of zno–aln pseudo-binary amorphous alloys with tunable band gaps in the deep ultraviolet region. Materials Research Express, 11(6), 065901.

Üzar, N. (2024). Enhancement of structural, optical, electrical, optoelectronic and thermoelectric properties of ZnO thin film via Ni doping and Ni-B co-doping. Physica Scripta, 99(7), 075995.

Yüksel, P., Hardal, G., & Kınacı, B. (2022). Influence of v2o5 and b2o3 addition on the sintering behaviour and physical properties of zno ceramics. Processing and Application of Ceramics, 16(1), 48-54.

Zhang, J., Tse, K., Wong, M., Zhang, Y., & Zhu, J. (2016). A brief review of co-doping. *Frontiers of Physics*, *11*(6). https://doi.org/10.1007/s11467-016-0577-2

Zhao, X., Jheng, J., Chou, N., Wang, F., & Yang, C. (2023). Synthesis of zno nanoflower arrays on a protrusion sapphire substrate and application of al-decorated zno nanoflower matrix in gas sensors. Sensors, 23(12), 5629.